Applied Physics Express

LETTERS

Highly sensitive torsion sensor based on directional coupling in twisted photonic crystal fiber

Applied Physics Express **11**, 042501 (2018)
https://doi.org/**10.7567/APEX.11.042501**

Highly sensitive torsion sensor based on directional coupling in twisted photonic crystal fiber

Feng Zhang, Shen Liu, Ying Wang*, Yijian Huang, Xizhen Xu, Cailing Fu, Tiesheng Wu, Changrui Liao, and Yiping Wang*

Key Laboratory of Optoelectronic Devices and Systems of Ministry of Education and Guangdong Province, College of Optoelectronic Engineering, Shenzhen University, Shenzhen 518060, China

*E-mail: yingwang@szu.edu.cn; ypwang@szu.edu.cn

Received December 14, 2017; accepted February 26, 2018; published online March 14, 2018

We demonstrate a novel torsion sensor based on a twisted photonic crystal fiber with an embedded liquid rod waveguide. Only one resonant dip appears in the transmission spectrum in the range of 1,350–1,650 nm, which is associated with the directional coupling between the core and rod modes. The relative position of the fiber core with respect to the liquid rod waveguide is altered owing to the torsion stress, which changes the phase-matching condition and leads to a resonant-wavelength shift. The helical structure of the liquid rod waveguide can improve the torsion sensitivity of the device and provide an ability to distinguish the rotation direction. The measured torsion sensitivities were as high as ~203 and ~208 nm·mm·rad^{-1} in the clockwise and counterclockwise rotations, respectively.

Highly sensitive torsion measurements using an optical fiber sensor have been employed in many applications,[1] such as anthropomorphic robotics, automotive industry, and security monitoring of buildings. Most reports on torsion sensors are based on long-period fiber gratings (LPFGs),[2,3] fiber Bragg gratings (FBGs),[4] and Sagnac interferometers.[5,6] However, many of these devices cannot distinguish the orientation of the applied torsion, which is disadvantageous for many practical applications. In recent years, helical structures in optical fibers have been investigated by many groups.[7–10] In the case of a loaded torsion stress, the helical pitch can be effectively reduced or enlarged, which makes the torsion orientation distinguishable. Structurally induced helical LPFGs in solid-core photonic crystal fibers (PCFs) have been reported, with potentials for applications in vectorial torsion sensing.[11,12] One of the most promising advantages of PCFs are the air holes arranged in the fiber cladding, which provide a platform for optical material infiltration and enable the creation of embedded satellite waveguides.[13,14] Various techniques of selective filling of PCFs have been developed and employed to fabricate fiber sensors with extremely high sensitivities,[15,16] which can also be employed to realize highly sensitive structures for torsion sensing.

In this study, we developed a sensitive torsion sensor based on twisted PCFs with an embedded waveguide structure, formed by a homogeneous rotation of the PCF under oxyhydrogen flame exposure and successive filling of one air hole of the twisted PCF with a refractive-index (RI) liquid. A lossy dip can be observed in the transmission spectrum owing to the coupling between the fiber core mode and liquid rod mode. The resonant wavelength can be tuned at approximately 1,550 nm by choosing an appropriate RI liquid. Experimental results show that the device exhibits a very high sensitivity of ~203 nm·mm·rad^{-1} in the clockwise rotation and ~208 nm·mm·rad^{-1} in the counterclockwise rotation.

PCFs (NKT Photonics ESM-12) with a hole diameter of ~3.6 μm and interhole spacing of ~7.9 μm were used in the experiments. Figure 1 shows the setup employed to fabricate the twisted PCFs. One side of the PCF was fixed by a fiber holder, while the other side was fixed on a rotator. The fiber holder and rotator were fixed onto two motorized linear translation stages, which were well aligned on an optical table.

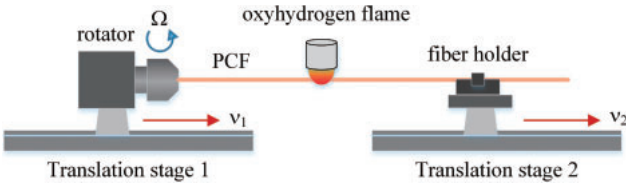

Fig. 1. Illustration of the setup for PCF twisting.

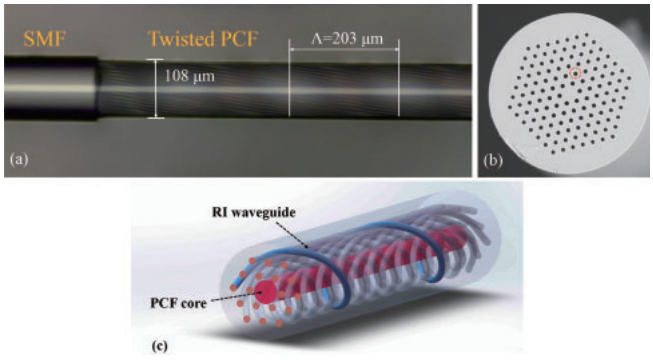

Fig. 2. (a) Side-view photograph of the SFTPCF spliced with an SMF. (b) Cross-section of the SFTPCF, where the red dotted circles outline the hole filled with a standard RI liquid. (c) Illustration of the SFTPCF (non-scaled) comprising a central solid core and helical liquid rod waveguide.

The oxyhydrogen flame heated the stripped PCF, and the rotator simultaneously operated to twist the PCF. In order to keep the fiber straight during the twisting process, the translation speed of the fiber holder (ν_2) was set to be slightly higher than that of the rotator (ν_1). The entire fabrication process was computer-controlled. It is worth noting that the rotation speed (Ω) of the rotator and translation speed of the translation stage determine the twisting period (T) of the fiber, which can be estimated using an experiential equation, $T = \nu_2/\Omega$. In the case of twisting a PCF with hexagonally arranged air holes, the twisting pitch (Λ) was reduced to $T/6$ owing to the sixfold symmetry. In our experiments, ν_1 and ν_2 were set to 1.38 and 1.6 mm/s, respectively. The left end of the fiber was twisted with a constant rate of $\Omega = 80$ rpm. As shown in Fig. 2, the twisting pitch of the sample was measured to be ~203 μm, which is approximately equal to the calculated result according to $\Lambda = T/6$. The diameters of the twisted PCF

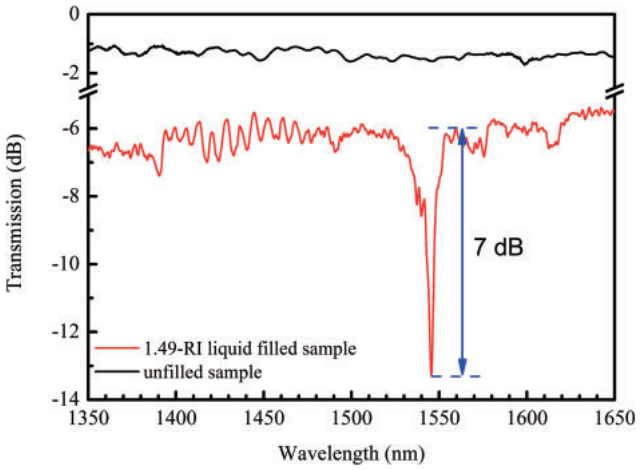

Fig. 3. Measured transmission spectra of the unfilled twisted PCF and 1.49-RI-liquid-filled twisted PCF.

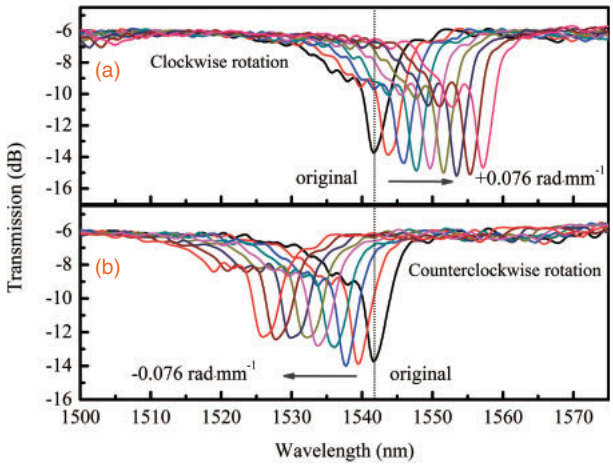

Fig. 4. Resonant-wavelength shifts of the SFTPCFs under an applied torsion in the range of -0.076 to $+0.076\,\mathrm{rad{\cdot}mm^{-1}}$ in steps of $0.0095\,\mathrm{rad{\cdot}mm^{-1}}$.

and air hole decreased to 108 and 2.7 µm, respectively, owing to the velocity difference (0.22 mm/s) between ν_1 and ν_2.

As shown in Fig. 2(b), one of the air holes located in the cladding of the twisted PCF was selectively filled with a 1.49-RI liquid using a femtosecond-laser-assisted selective filling method.[17] The selectively filled twisted PCF (SFTPCF) sample is expected to exhibit an improved torsion sensitivity, as it combines the advantages of helical structures and embedded directional coupler in the PCF. In Fig. 2(c), the three-dimensional (3D) geometry (non-scaled) of the SFTPCF shows that the RI liquid rod can form a waveguide in the air hole and wrap around the PCF core.

In general, in twisted solid-core PCFs, the resonant dips in the transmission spectrum originate from the resonant coupling between the PCF core mode and cladding modes, as observed in LPFGs.[18] In order to obtain a unique dip for tracing, we increased the twisting period of the PCF to avoid the dips resulting from the LPFG. A series of twisted PCF samples with different periods were prepared; transmission spectra were recorded until no apparent resonant dips could be observed. A PCF sample with a twisting period of 1,200 µm and twisting rate (α_0) of $5.2\,\mathrm{rad{\cdot}mm^{-1}}$ satisfied this requirement.

The twisted PCF was then spliced with a section of a single-mode fiber (SMF) that was cut off, and only a 10-µm-long SMF was preserved. One hole in the cladding was drilled from the cross-section of the SMF using a femtosecond-laser beam. The selectively opened end of the twisted PCF was immersed into the RI liquid; the liquid filled the opened hole of the twisted PCF owing to the capillary force. A filled sample with a twisted section length of 4.2 cm was prepared; both ends of the sample were fusion-spliced with an SMF and connected to a super-continuum light source (NKT Photonics Super K Compact) and optical spectrum analyzer (Yokogawa Test and Measurement AQ6370C), respectively.

The transmission spectrum of the twisted PCF sample is plotted in Fig. 3. In the wavelength range of 1,350–1,650 nm, no obvious lossy dips can be observed in the spectra of the unfilled sample (black curve), which indicates that no resonant dip of the LPFG is formed, implying that the method of fabricating twisted PCFs is reliable. The same twisted PCF was then used to prepare a selectively filled sample. The spectrum of this sample shows an apparent resonant dip at approximately 1,550 nm, which originates from the coupling between the fiber core mode and liquid rod mode. The strength of the directional coupling resonance is ~7 dB. The strength of the weak interference fringes caused by the splicing joints between the twisted PCF and SMF is ~1 dB, which does not interfere with the performance of this device. The resonant dip is sufficiently unique to be traced for torsion tests.

The novel device was placed in a torsion test system[19] to observe the shift of the resonant dip with the increase of the torsion angle. One rotator was fixed, while the other one was rotated in the clockwise (+) or counterclockwise (−) directions, which were equal to or opposite to the direction of the twisting PCF, respectively. The distance (L) between the two fiber holders was 55 mm. Therefore, the applied torsion τ can be estimated by $\tau = \theta/L$ ($\mathrm{rad{\cdot}mm^{-1}}$). It is worth noting that the device is highly sensitive to temperature. In order to eliminate the temperature influence, the device was covered under a protective shield, which maintained the sample at a constant temperature of 22 °C during the torsion test, yielding stable spectra.

The unique resonant dip could be traced in the spectra, where the angle of rotation (θ) was varied from 0 to ±240° ($\pm 0.076\,\mathrm{rad{\cdot}mm^{-1}}$ in this case), in intervals of 30° ($0.0095\,\mathrm{rad{\cdot}mm^{-1}}$). Larger rotation angles were not applied to avoid damage to the fiber. A series of spectral responses for different angles of rotation is plotted in Fig. 4. It is evident that the resonant dip shifts to the opposite direction when the sample is rotated oppositely. The SFTPCF can distinguish opposite rotations without the need for pre-twisting owing to the helical structure.

It is well known that mode coupling can only occur around the phase-matching point, where the effective RI of the core mode overlaps with that of the rod waveguide mode. The shift of the phase-matching point is mainly caused by the relative position change of the liquid rod waveguide with respect to the fiber core with the rotation. As shown in Fig. 5, when the SFTPCF rotates, the angle (Φ) between the liquid rod waveguide and fiber core changes, which can be expressed as[20]

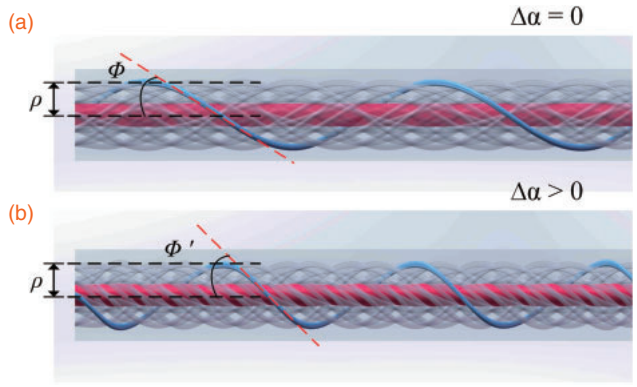

Fig. 5. Illustration of the local fiber core and liquid rod waveguide in the SFTPCF during the torsion test. (a) Non-rotated sample ($\Delta\alpha = 0$). (b) Sample rotated in the clockwise direction ($\Delta\alpha > 0$).

$$\Phi = \sin^{-1}[\alpha\rho/(1+\alpha^2\rho^2)^{0.5}] \approx \alpha\rho, \quad (1)$$

where α is the twist rate, and ρ is the spacing between the fiber core and liquid rod waveguide. The coupling condition can be derived by

$$n_{\mathrm{rod}}\rho^2\alpha = l\frac{\lambda_{\mathrm{R}}}{2\pi}, \quad (2)$$

where n_{rod} is the effective refractive index of the liquid rod waveguide, l is an integer representing the order of the resonance, and λ_{R} is the resonant wavelength. The product $n_{\mathrm{rod}}\rho^2$ is a constant for a given PCF.[20] This equation shows that λ_{R} depends linearly on the fiber twist rate α; it shifts towards longer wavelengths with the increase of α.

During the torsion test, when the direction of rotation was equal to that of the PCF twisting, under a torsion stress, the angle Φ between the fiber core and liquid rod waveguide increased (Fig. 5), which implies that the twist rate α improved with a constant ρ. According to Eq. (2), the resonant wavelength λ_{R} shifted towards longer wavelengths. However, when the rotation was in the direction opposite to that of the PCF twisting, the angle Φ and twist rate α were decreased by the torsion stress, which caused the blue-shift of the resonant wavelength.

The wavelength variation of the lossy dip with the applied torsion (τ) is plotted in Fig. 6 to demonstrate the linear operation of the device. As shown in the figure, average torsion sensitivities of ~203 and ~208 nm·mm·rad^{-1} in the clockwise and counterclockwise rotations, respectively, are calculated and obtained. They are approximately 4 times higher than those of the helical PCF,[11] which exhibits sensitivities of 56 nm·mm·rad^{-1}, and over 10 times higher than those of conventional LPFGs.[19] The linearities of the fitting curves are both up to 0.99, which indicates that the torsion sensor can be easily demodulated.

The torsion sensitivity of a selectively filled untwisted PCF (SFUPCF) was also investigated in order to compare it with those of the twisted PCF. The preparation method of the SFUPCF is identical to that of the SFTPCF, except that there is no twisting process. The transmission spectra of the SFUPCF at different torsion angles were measured. The inset of Fig. 7 shows the transmission spectra of the UPCF without torsion. Two resonant dips were observed at approximately 1,285 and 1,300 nm, owing to the coupling between the PCF's fundamental core mode and rod's higher-order modes.[21] However, unlike a twisted PCF, it is very challenging to distinguish between clockwise and counterclockwise torsions by the shift of resonant dips, as shown in Fig. 7. An obvious wavelength shift is not observed between the two opposite torsion directions.

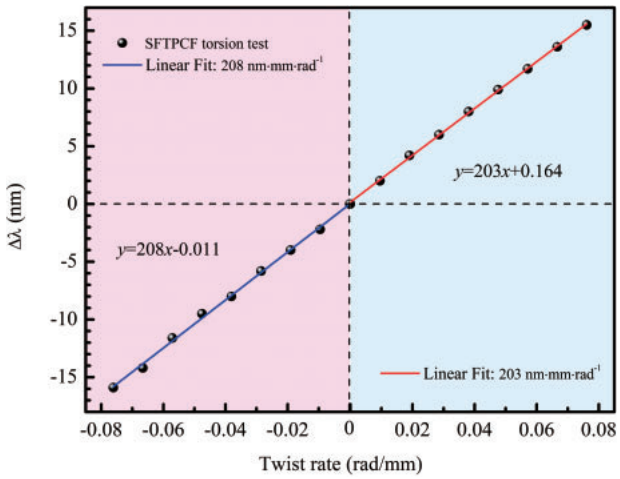

Fig. 6. Linear fitting between the torsion and wavelength shift for the SFTPCF.

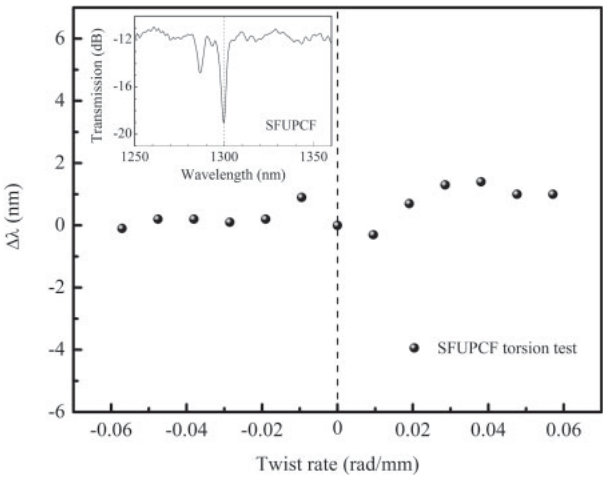

Fig. 7. Dip wavelengths of the SFUPCF device at torsions in the range of −0.06 to +0.06 rad·mm^{-1} in steps of 0.0095 rad·mm^{-1}.

In conclusion, we proposed a novel fiber device based on an SFTPCF for torsion measurements. The operation principle of the device is based on the directional coupling between the fiber core mode and liquid rod mode. The shift of the resonant wavelength was caused by the change of the angle between the fiber axis and liquid rod waveguide. The measured torsion sensitivities were as high as ~203 and ~208 nm·mm·rad^{-1} in the clockwise and counterclockwise rotations, respectively. This device has significant potentials for ultra-sensitive torsion measurements.

Acknowledgments This study was supported by the National Natural Science Foundation of China (NSFC) (Grant Nos. 61705138, 61675137, 61425007, and 61635007), Guangdong Natural Science Foundation (Grant Nos. 2017A030310033, 2015B010105007, and 2014A030308007), China Postdoctoral Science Foundation (Grant No. 2016M600669), Science and Technology Innovation Commission of Shenzhen (Grant Nos. JCYJ20160307143716576, JCYJ20160307143501276, and JCYJ20160427104925452), Education Department of Guangdong Province (Grant No. 2015KTSCX119), and Development and Reform Commission of Shenzhen Municipality Foundation.

1) V. Budinski and D. Donlagic, Sensors **17**, 443 (2017).
2) L. A. Wang, C. Y. Lin, and G. W. Chern, Meas. Sci. Technol. **12**, 793 (2001).
3) Y. P. Wang, J. P. Chen, and Y. J. Rao, J. Opt. Soc. Am. B **22**, 1167 (2005).
4) F. Yang, Z. J. Fang, Z. Q. Pan, Q. Ye, H. W. Cai, and R. H. Qu, Opt. Express **20**, 28839 (2012).
5) B. B. Song, H. Zhang, Y. P. Miao, W. Lin, J. X. Wu, H. F. Liu, D. L. Yan, and B. Liu, Opt. Express **23**, 15372 (2015).
6) P. Zu, C. C. Chan, Y. X. Jin, T. X. Gong, Y. F. Zhang, L. H. Chen, and X. Y. Dong, IEEE Photonics Technol. Lett. **23**, 920 (2011).
7) V. I. Kopp and A. Z. Genack, Nat. Photonics **5**, 470 (2011).
8) L. A. Fernandes, J. R. Grenier, J. S. Aitchison, and P. R. Herman, Opt. Lett. **40**, 657 (2015).
9) K. Ren, L. Ren, Y. Wang, X. Lin, J. Liang, Y. Xu, and H. Ju, Opt. Laser Technol. **92**, 150 (2017).
10) H. L. Zhang, Z. F. Wu, P. P. Shum, X. Q. Dinh, C. W. Low, Z. L. Xu, R. X. Wang, X. G. Shao, S. N. Fu, W. J. Tong, and M. Tang, Sci. Rep. **7**, 10 (2017).
11) X. M. Xi, G. K. L. Wong, T. Weiss, and P. S. Russell, Opt. Lett. **38**, 5401 (2013).
12) W. Shin, Y. L. Lee, B. A. Yu, Y. C. Noh, and K. Oh, Opt. Commun. **282**, 3456 (2009).
13) B. T. Kuhlmey, B. J. Eggleton, and D. K. C. Wu, J. Lightwave Technol. **27**, 1617 (2009).
14) D. K. C. Wu, K. J. Lee, V. Pureur, and B. T. Kuhlmey, J. Lightwave Technol. **31**, 3500 (2013).
15) Y. Wang, M. Yang, D. N. Wang, and C. R. Liao, IEEE Photonics Technol. Lett. **23**, 1520 (2011).
16) C. P. Lin, Y. Wang, Y. J. Huang, C. R. Liao, Z. Y. Bai, M. X. Hou, Z. Y. Li, and Y. P. Wang, Photonics Res. **5**, 129 (2017).
17) Y. Wang, C. R. Liao, and D. N. Wang, Opt. Express **18**, 18056 (2010).
18) V. I. Kopp, V. M. Churikov, J. Singer, N. Chao, D. Neugroschl, and A. Z. Genack, Science **305**, 74 (2004).
19) M. Deng, J. Xu, Z. Zhang, Z. Bai, S. Liu, Y. Wang, Y. Zhang, C. Liao, W. Jin, G. Peng, and Y. Wang, Opt. Express **25**, 14308 (2017).
20) G. K. L. Wong, M. S. Kang, H. W. Lee, F. Biancalana, C. Conti, T. Weiss, and P. St. J. Russell, Science **337**, 446 (2012).
21) D. K. C. Wu, B. T. Kuhlmey, and B. J. Eggleton, Opt. Lett. **34**, 322 (2009).